PAPER

Check for updates

Defect and strain engineered MoS$_2$/graphene catalyst for an enhanced hydrogen evolution reaction†

Zhaoyuan Yang,[a] Jia Zhu, [ID] *[a] Xianglan Xu,[b] Lei Wang,[a] Guobing Zhou,*[a] Zhen Yang [ID] *[a] and Yongfan Zhang [ID] [c]

Molybdenum disulfide (MoS$_2$) has been demonstrated as a promising non-precious metal electrocatalyst for the hydrogen evolution reaction (HER). However the efficiency of the HER falls short of expectations due to the large inert basal plane and poor electrical conductivity. In order to activate the MoS$_2$ basal plane and enhance the hydrogen evolution reaction (HER) activity, two strategies on the hybrid MoS$_2$/graphene, including intrinsic defects and simultaneous strain engineering, have been systematically investigated based on density functional theory calculations. We firstly investigated the HER activity of a MoS$_2$/graphene hybrid material with seven types of point defect sites, V_S, V_{S2}, V_{Mo}, V_{MoS3}, V_{MoS6}, Mo$_{S2}$ and S2$_{Mo}$. Using the hydrogen adsorption free energy (ΔG_H) as the descriptor, results demonstrate that four of these seven defects (V_S, V_{S2}, Mo$_{S2}$, V_{MoS3}) act as a catalytic active site for the HER and exhibited superior electrocatalytic activity. More importantly, we found that ΔG_H can be further tuned to an ideal value (0 eV) with proper tensile strain, which effectively optimizes and boosts the HER activity, especially for the V_S, V_{S2}, V_{MoS3} defects and Mo$_{S2}$ antisite defects. Our results demonstrated that a proper combination of tensile strain and defect structure is an effective approach to achieve more catalytic active sites and further tune and boost the intrinsic activity of the active sites for HER performance. Furthermore, the emendatory d-band center of metal proves to be an excellent descriptor for determining H adsorption strength on defective MoS$_2$/graphene hybrid material under different strain conditions. In addition, the low kinetic barrier of H$_2$ evolution indicated that the defective MoS$_2$/graphene system exhibited favorable kinetic activity in both the Volmer–Heyrovsky and the Volmer–Tafel mechanism. These results may pave a new way to design novel ultrahigh-performance MoS$_2$-based HER catalysts.

1. Introduction

The process of electrochemical water splitting to produce hydrogen energy *via* the hydrogen evolution reaction (HER) has been considered a renewable, green, and highly efficient technique. Pt and Pt-group metals are regarded as the best catalysts for the hydrogen evolution reaction (HER).[1] However, these metals are a limited natural resource, which significantly elevates the cost of using these metals, thereby limiting their utilization in practice. These major issues make it essential to develop a naturally abundant and inexpensive material with

highly active HER performance as an alternative to Pt, but has remained a challenge thus far.

Recently, molybdenum disulfide (MoS$_2$) has attracted a large amount of attention as a promising non-precious metal catalyst for the hydrogen evolution reaction (HER). MoS$_2$ is low-cost, naturally abundant, has high chemical stability, and a comparable catalytic HER performance to Pt.[2,3] However, MoS$_2$ HER efficiency does not meet expectations because the catalytic activity of MoS$_2$ highly depends on its active edge sites, thereby rendering the large inert basal plane non-catalytic, as well as a poor electrical conductivity for the catalyst.[4] Many strategies are being explored to optimize the catalytic performances of MoS$_2$, including controlling the size of MoS$_2$ to expose more active edge sites using nanoparticles,[5] nanowires,[6] nanoflakes[7] and nanotube,[8] as well as coupling MoS$_2$ with other conductive scaffolds, such as graphene,[9,10] carbon nanotube[11] and Au electrode,[12] to improve electrical conductivity of MoS$_2$ material and HER electrocatalytic activity. Chemical doping[13] and defects formation[14,15] are two additional methods used to improve the intrinsic active sites. Voiry *et al.* reported that the catalytic activity of the 2H-MoS$_2$ basal plane was significantly enhanced

[a]*Key Lab of Fluorine and Silicon for Energy Materials and Chemistry of Ministry of Education, College of Chemistry and Chemical Engineering, Jiangxi Normal University, Nanchang 330022, China. E-mail: jia_zhu@jxnu.edu.cn; gbzhou@jxnu. edu.cn; yangzhen@jxnu.edu.cn*

[b]*Institute of Applied Chemistry, College of Chemistry, Nanchang University, Nanchang, Jiangxi, 330031, China*

[c]*College of Chemistry, Fuzhou University, Fuzhou, Fujian, 350108, China*

† Electronic supplementary information (ESI) available: See DOI: https://doi.org/10.1039/d2ra07363c

when the presence of sulfur vacancies were combined with an efficient charge injection between the conductive Au support and the catalyst.[12] Using argon plasma exposure, Tsai *et al.* have shown that S-vacancies on 2H-MoS$_2$ exhibited higher intrinsic activity in HER than at the edge sites.[15]

Recent research has additionally found that tuning strain is a powerful strategy for tailoring the catalytic activity to achieve the highest intrinsic HER activity.[16–18] The application of external strain on the 1T$'$-MX$_2$ (M = Mo, W; X = S, Se, Te) significantly tunes and boosts the HER performance.[19] Li *et al.* have reported that introducing strain on the S vacancy-MoS$_2$ basal plane could enormously enhance its HER activity.[20] Dimakis *et al.* have also examined the S, S$_2$ vacancies and C vacancies in the MoS$_2$/graphene heterostructure could be engineered for producing efficient HER electrocatalysts based on density functional theory (DFT), but the reaction model by combining the molecular dynamics (MD) simulations are not considered.[21,22] Recently, experimentation has systematically identified a variety of intrinsic defects prepared by chemical vapor deposition (CVD) grown monolayer MoS$_2$.[23,24] However, it is still unknown what potential roles would various combinations of the different intrinsic defects and engineered strains play on the HER performance of MoS$_2$-based materials. It prompted us to investigate if strain engineering and different intrinsic defects simultaneously could increase both the number of active sites and intrinsic catalysis activity, thus exhibiting significantly enhanced HER performance for MoS$_2$-based hybrid materials.

In this study, we explored both the strain engineering and intrinsic defect strategies to optimize the hydrogen evolution reaction (HER) catalytic activity of the MoS$_2$ basal plane grown on graphene using the first-principles DFT calculation. Used 7 different types of point defects commonly observed in experiments includes a monosulfur vacancy (V_S), a disulfur vacancy (V_{S2}), an Mo vacancy (V_{Mo}), a vacancy complex of Mo and three nearby sulfur (V_{MoS3}), a vacancy complex of Mo and six nearby sulfur (V_{MoS6}), antisite defects where an Mo atom substitutes for an S$_2$ column (Mo$_{S2}$) and an S$_2$ column substitutes for an Mo atom (S2$_{Mo}$). Our results show that MoS$_2$/graphene hybrid with intrinsic defects can activate the inert basal plane and greatly improve the HER activity. Furthermore, we found significant improvement of the HER intrinsic activity of the active site for the MoS$_2$/graphene hybrid material when we use a combination of a defect structure and a proper strain. Our results may pave an effective strategy to design ultrahigh-performance MoS$_2$-based HER catalysts.

2. Computational methods

2.1. Model systems

The optimized lattice parameters of monolayer MoS$_2$ and graphene were calculated to be 3.17 Å and 2.46 Å, respectively, which is well in agreement with the experimental and theoretical results.[25–27] The supercell structure of the composite system is (4 × 4) MoS$_2$ and (5 × 5) graphene, which includes about a 2.9% lattice mismatch. The lattice of graphene was initially set to match that of monolayer MoS$_2$ in the supercell, and then the

supercells fully relaxed for both the lattice constants and the atomic geometry. Eventually, the mismatch would finally disappear, leading to the commensurate systems. The relaxed lattice constants of the MoS$_2$/graphene system is approximately 12.44 Å. The lattice of parameter of MoS$_2$ layer in the supercell are slightly compressed by 1.9% (from 3.17 Å to 3.11 Å) when compared to the corresponding isolated sheet, while the graphene layer in the supercells are slightly expanded by 1.2% (from 2.46 Å to 2.49 Å).The lattice constants experienced a slight decrease for defective MoS$_2$(V_S, V_{S2}, V_{MoS3}, V_{MoS6}, Mo$_{S2}$)/graphene systems, while lattice constants for V_{Mo}-MoS$_2$/graphene and S2$_{Mo}$-MoS$_2$/graphene systems remained mostly unchanged, both with respect to a perfect MoS$_2$/graphene system. The monolayer MoS$_2$ have the direct band gap of 1.73 eV at the *k* point. While for MoS$_2$/graphene, a tiny band gap of about 2 meV is opened in the Dirac cone of graphene. It is indicated that the combination of the chemically inert graphene with MoS$_2$ as van der Waals heterostructure provides better electron conduction and ion transportation, result in improvement of the electrocatalytic performance (Fig. S1†).

The reaction mechanism was investigated by constructing a solid/liquid interfacial model, which was modeled with the substrate covered by two water layers. The water–solid interface was obtained by combining the molecular dynamics (MD) simulations and structural optimization. Molecular dynamics (MD) simulations were initially performed using the LAMMPS package to equilibrate the structure of water molecules at the interface of monolayer MoS$_2$.[28] The rectangular supercell of monolayer MoS$_2$ had a rectangular dimension of approximately 21.545 × 24.878 Å^2 in *x* and *y* direction, respectively, and a water film initially placed on the top of the surface contained a total number of 538 H$_2$O molecules. Periodic boundary conditions were applied in all three directions and a vacuum 5.0 nm thick was added above the water film to prevent interactions between the periodic images. We employed the flexible extended simple point charge (SPC/E) model[29] for the water solvent and maintained a fixed surface structure during the simulation. The employed force field for MoS$_2$ was developed by Heiranian *et al.*,[30] which has been demonstrated to reproduce excellent water–MoS$_2$ interface properties. The cutoff distance for the non-bonded interactions was set to be 10.0 Å, and the long-range electrostatic interactions were calculated using the particle-particle particle-mesh method (PPPM).[31] The canonical ensemble (NVT) was applied during the simulation, temperature was held at 300.0 K *via* the Nose-Hoover method, and the coupling coefficient was 0.1 ps. The entirety of the simulation was completed in 20.0 ns, where the first 10.0 ns was for equilibrium and the remaining 10.0 ns were used for data collection. Afterwards, the interface water molecules were first extracted from the equilibrium structure and then a hexagonal cell was cleaved from the obtained structure (see Fig. S2†), which was used for the subsequent DFT calculations. The dimension of the monolayer MoS$_2$ is 12.44 × 12.44 Å^2 and there are totally 32 water molecules on the surface. Proton concentration can be changed when hydrogen atoms are added into the systems. The H atom forms proton either through being adsorbed on the surface or solvated in the water layer. The water–solid interfaces

with two layers of proton-laden water molecules were used to simulate the electrical double layer in an acid solution.

2.2. Computational methods

Spin-polarized density functional theory (DFT) calculations were carried out using the Vienna *ab initio* simulation package (VASP).[32–34] The projector augmented wave method was certified to describe the interaction between electrons and ions,[35] and the generalized gradient approximation (GGA) of the Perdew–Burke–Ernzerhof (PBE) functional exchange-correlation functional was employed.[36] The pseudopotentials with $4p_6 5s_1 4d_5$, $3s_2 3p_4$, $2s_2 2p_2$ and $1s_1$ are used for Mo, S, C and H atoms here under PAW, respectively. The kinetic cutoff energy for the plane-wave expansion was set to 500 eV. The spacing between the adjacent slabs was set to about 15 Å, and a $(5 \times 5 \times 1)$ Monkhorst–Pack mesh was used for the k-point sampling of the Brillouin zone. DFT-D3 calculations were used to describe the weak interactions.[37] During structural optimization, all the internal coordinates were fully relaxed in all directions. The HER activity of the catalyst was evaluated by calculating the free energy of the adsorption atomic hydrogen (ΔG_H), which can be obtained by $\Delta G_H = \Delta E_H + \Delta E_{ZPE} - T\Delta S_H$. The ΔE_H presents the adsorption energy of the nth H atom, which is defined as: $\Delta E_H = E_{MoS2/graphene+nH} - E_{MoS2\text{-}graphene+(n-1)H} - 1/2\, E_{H2}$, where $E_{MoS2\text{-}graphene+nH}$ and $E_{MoS2\text{-}graphene+(n-1)H}$ represents the total energy of the MoS_2/graphene system with n and $n-1$ adsorbed H atoms on the surface, respectively, while E_{H2} represents the total energy of H_2 in gas phase. The ΔE_{ZPE} is the zero-point energy difference between the adsorbed state of the different defective MoS_2/graphene system and the gas-phase state, the ΔS_H is obtained by $\Delta S_H \cong -1/2\, S^0_{H2}$, and the S^0_{H2} is the entropy of H_2 in gas phase at standard condition ($S^0_{H2} \sim 130$ J mol K^{-1}).[38] The diffusion energy barrier and the minimum energy pathways for H_2 evolution were determined using the climbing-image nudged elastic band (CI-NEB) method,[39] and each transition state was further confirmed by vibrational frequency analysis.

3. Results and discussion

3.1. Gibbs free energy (ΔG_H) of atomic hydrogen on MoS_2-graphene system with the different intrinsic defects and strain engineering

We first studied the HER activity of the MoS_2/graphene hybrid material with different intrinsic defects(V_S, V_{S2}, V_{Mo}, V_{MoS3}, V_{MoS6}, Mo_{S2} and $S2_{Mo}$, respectively). We started with various possible adsorption sites on MoS_2-graphene system for a single H atom with each intrinsic defects were considered. The most stable adsorption configurations are shown in Fig. 1. Results show that after different intrinsic defects are introduced, the binding of the H atom with the defective MoS_2/graphene hybrid materials stabilizes. The H atom showed location preference at the S vacancy for the MoS_2/graphene system with the V_S and V_{S2} defects, and with the Mo_{S2} defects, the H atom showed preference to bond with one Mo atom. The H atom connected the bridge site between two Mo atoms with the V_{MoS3} and V_{MoS6} defects, but with V_{Mo} and $S2_{Mo}$ defects, the H atom interacted

with top site of S atom instead with Mo site. The Gibbs free energy for hydrogen adsorption on a catalyst surface (ΔG_H) has been demonstrated to be a good descriptor for HER activity, as shown in Nørskov's analyses.[40] An ideal ΔG_H on catalyst should be close to 0 eV where hydrogen is bonded neither too strongly nor too weakly. Therefore, we calculated the single H atom adsorption free energy (ΔG_H) for MoS_2/graphene system with different intrinsic defects(V_S, V_{S2}, V_{Mo}, V_{MoS3}, V_{MoS6}, Mo_{S2} and $S2_{Mo}$), as shown in Fig. 2A. The result show that after different intrinsic defects (V_S, V_{S2}, V_{Mo}, V_{MoS3}, V_{MoS6}, Mo_{S2} and $S2_{Mo}$) are introduced, the calculated ΔG_H for each defect is much lower than the defect-free basal plane (1.9 eV),[41] indicating that intrinsic defects can bring additional active site and trigger HER activity of the inert basal plane. This finding agrees with previous experimental studies, where the active sites were the vacancies created on the 2H-MoS_2.[15] For the case of V_{MoS6}, the calculated ΔG_H is very negative, demonstrating that the interaction is too strong to ensure a facile bond breaking and the release of gaseous H_2. It is worth noting that the ΔG_H for V_S, V_{S2}, V_{MoS3} and Mo_{S2} defects is only 0.04 eV, 0.09 eV, −0.14 eV and −0.07 eV, respectively, which was close to an ideal value (0 eV). It is indicated that these 4 kinds of defects have highly catalytic activity for the Volmer reaction. These values are approximate to or are better than the Pt value (−0.09 eV) or Mo edge (0.08 eV),[3] indicating that defective MoS_2/graphene system had higher intrinsic HER activity with the V_S, V_{S2}, V_{MoS3} and Mo_{S2} defects. We have examined the sub-layer effect on the defective MoS_2/graphene systems at different strain engineering. We found that, after H adsorption on the defective MoS_2/graphene system, the Mo-Mo distance and the length of Mo–S bond between sub-layer Mo atom and top layer S atom around the defect are changed a little. It is indicated that the energy cost induced by structural changes with H adsorption are very small. The result is also agreement with the further investigation of the calculated structure reconstruction energy (ΔE_R) for all the different defective MoS_2/graphene systems, which is the energy cost induced by structural changes with H adsorption. We calculated the energy of structural reconstruction, ΔE_R, by subtracting the energy of the adsorption structure with H removed from the energy of the clean structure without H adsorption. Except for the V_{MoS3} defect, it is can be seen that, values of ΔE_R are very small for the defective MoS_2/graphene systems, suggesting that the defective MoS_2/graphene systems can retain good structural stability during the hydrogen adsorption and release.

Next, we explored whether intrinsic defects and strain engineering simultaneously could bring better HER activity for MoS_2/graphene hybrid material. We further explored the effects of biaxial strain on these defective MoS_2/graphene with a series of intrinsic defects(V_S, V_{S2}, V_{Mo}, V_{MoS3}, V_{MoS6}, Mo_{S2} and $S2_{Mo}$). Fig. 2B and C display a variation in ΔG_H under biaxial strains ranging from −5 to +5% for seven kinds of defective MoS_2-graphene system by varying the lattice parameters (Fig. 1). As evident in Fig. 2, it is interesting to note that the defects have different responses to strain. As for the MoS_2/graphene system with V_S, V_{S2}, V_{MoS3} and Mo_{S2} defects (Fig. 2B), under biaxial strains ranging from −5 to +5%, they achieved the ideal value of ΔG_H of approximately 0 eV at 1%, 1%, 4% and 1% tensile strain,
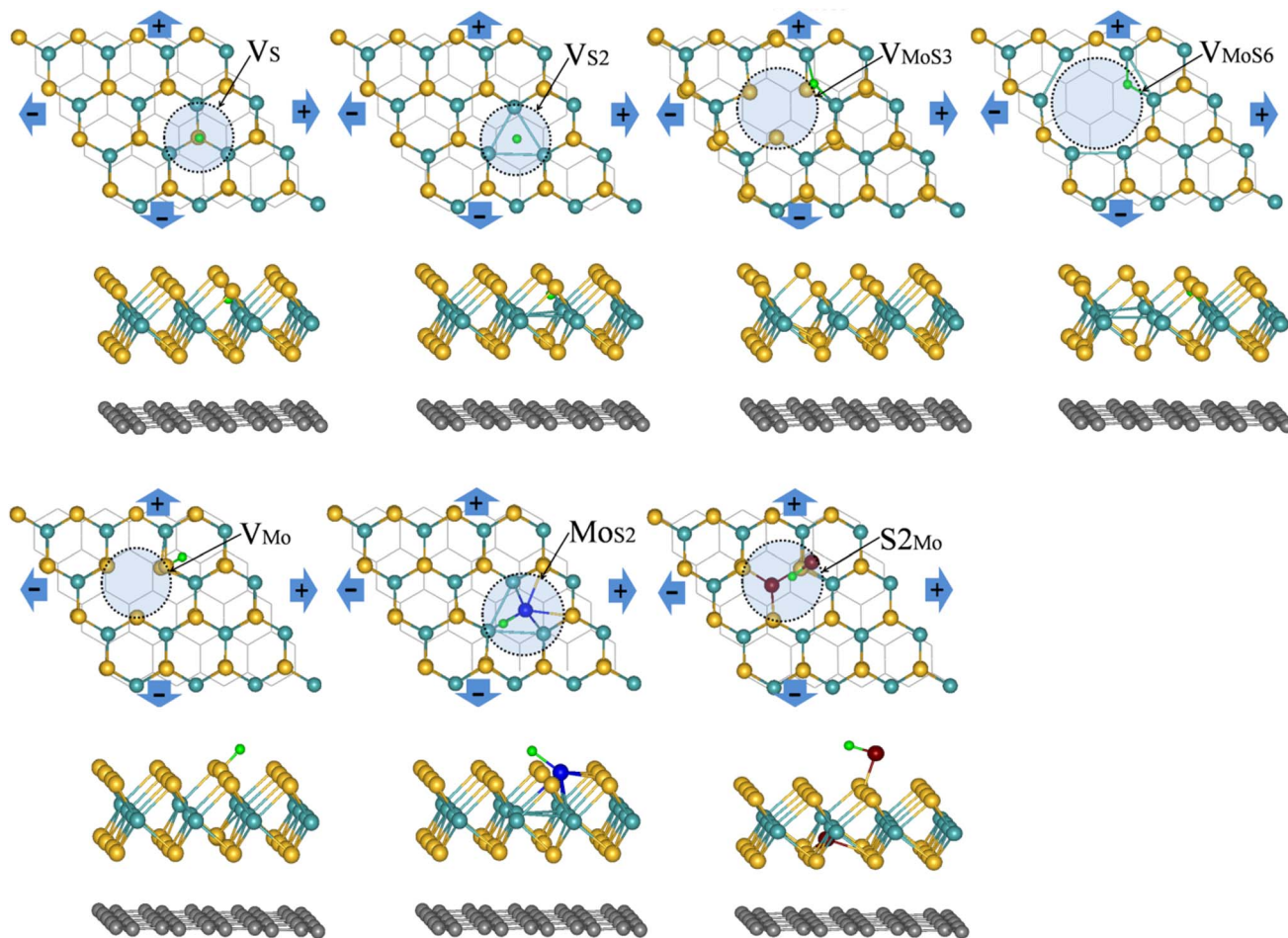
Fig. 1   The top and side views of the most stable position for single H atom adsorbing at MoS_2/graphene system with different intrinsic defects (V_S, V_{S2}, V_{MoS3}, V_{MoS6}, V_{Mo}, Mo_{S2} and $S2_{Mo}$, respectively) at strain engineering. The yellow, cyan and green balls present S, Mo and H atoms, respectively, the brown and dark blue balls stand for atom replaced by S and Mo atoms respectively, the bottom black line or balls refer to the graphene.

respectively. It is indicated the V_S, V_{S2}, V_{MoS3} and Mo_{S2} defects particularly had optimal responses to different tensile strains with optimal ΔG_H values ($\sim$0 eV) and effectively tune and boost

the intrinsic activity of defective MoS_2/graphene hybrid materials. In contrast, for the MoS_2/graphene hybrid with the V_{Mo}, V_{MoS6} and $S2_{Mo}$ defects (Fig. 2C), when applying biaxial strains
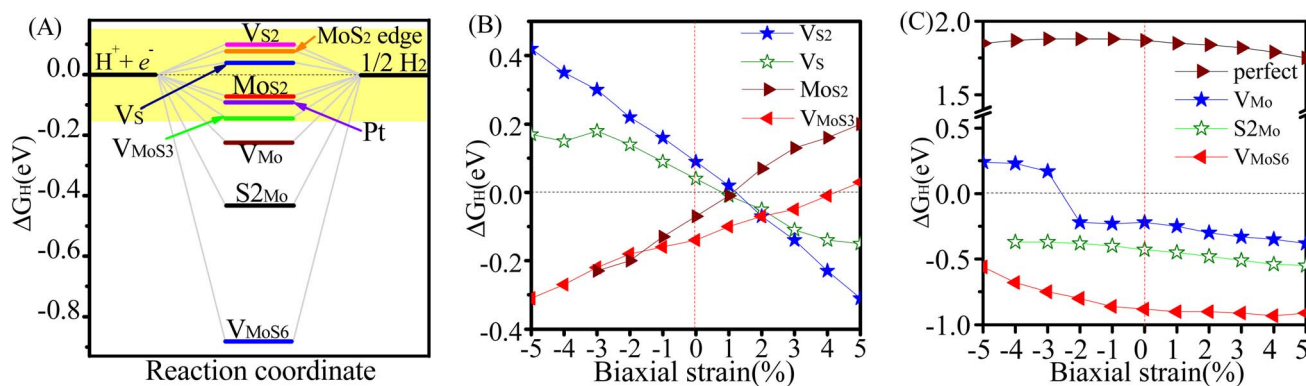
Fig. 2   (A) ΔG_H for HER on MoS_2/graphene catalysts with different intrinsic defects (V_S, V_{S2}, V_{Mo}, V_{MoS3}, V_{MoS6}, Mo_{S2}, $S2_{Mo}$), MoS_2 edge and Pt, respectively. The result of Pt catalyst and MoS_2 edge is taken from ref. 3. (B) ΔG_H for HER on MoS_2/graphene catalysts with different intrinsic defects (V_S, V_{S2}, V_{MoS3}, Mo_{S2}) versus %x-biaxial strain ranging from −5 to +5%. (C) ΔG_H for HER on perfect MoS_2/graphene and MoS_2/graphene systems with different intrinsic defects (V_{Mo}, $S2_{Mo}$, V_{MoS6}) versus %x-biaxial strain ranging from −5 to +5%.
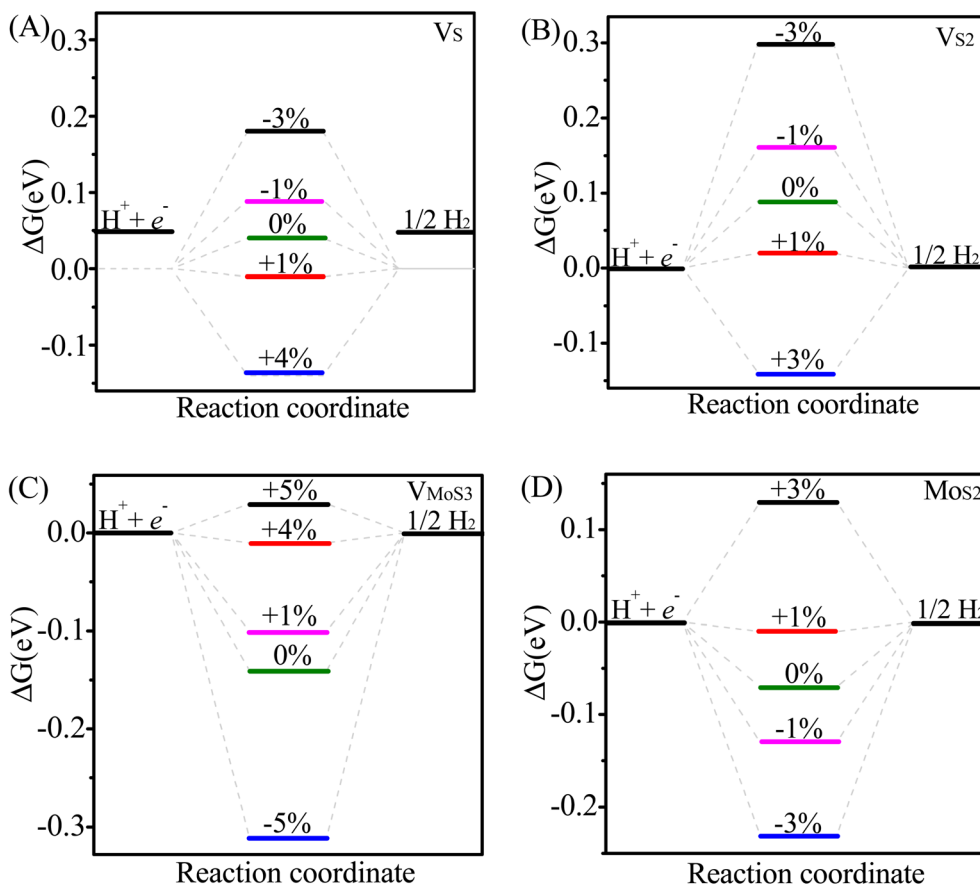
Fig. 3 Effect of strain on the HER performance of different MoS$_2$/graphene catalysts with different intrinsic defects (V_S, V_{S2}, V_{MoS3}, Mo$_{S2}$): free energy(ΔG_H) diagram for the HER on different catalysts at different strain: (A) V_S-MoS$_2$/graphene, (B) V_{S2}-MoS$_2$/graphene, (C) V_{MoS3}-MoS$_2$/graphene, (D) Mo$_{S2}$-MoS$_2$/graphene.

for either positive strain (tensile strain) or negative strain (compressive strain), although there is moderate drop in ΔG_H, the ΔG_H are all larger than |0.22 eV|, |0.5 eV| and |0.3 eV|, respectively, proved insufficient to optimize HER activity of the MoS$_2$/graphene hybrid with the V_{Mo}, V_{MoS6} and S2$_{Mo}$ defects, responses to biaxial strains. Fig. 3 further shows the effect of strain on hydrogen binding free energy with V_S–MoS$_2$/graphene, V_{S2}–MoS$_2$/graphene, V_{MoS3}–MoS$_2$/graphene and Mo$_{S2}$–MoS$_2$/graphene. It can be seen clearly, there was a negative strain (compressive strain) for the V_S defect with a 3% increase of the ΔG_H to 0.18 eV. It is noteworthy that, a small positive strain (tensile strain) of 1% dropped ΔG_H to −0.01 eV, which is very close to the ideal value of ΔG_H (0 eV). It is indicated hydrogen adsorption was significantly stronger and subsequently HER activity improved. Interestingly, in the absence of strain, the ΔG_H was calculated at 0.09 eV in V_{S2}-MoS$_2$/graphene system. Biaxial tensile strain tends to lower the ΔG_H. It appeared to catch up with that case of V_S defect and eventually become significantly more active at modest tensile strain (1%) with the ideal value of ΔG_H of approximately 0 eV, which is the best value for potential HER activity (Fig. 2B). The ΔG_H and H adsorption strength of MoS$_2$/graphene hybrid with V_{MoS3} and Mo$_{S2}$ defect also showed sensitivity to biaxial strain. However, biaxial tensile strain tended to weaken hydrogen adsorption for V_{MoS3} and

Mo$_{S2}$, which differed from the V_S and V_{S2} defect, where which biaxial tensile strain strengthened the hydrogen adsorption. The V_{MoS3} and Mo$_{S2}$ defect achieved a more favorable ΔG_H (close to 0) at 4% and 1% tensile strain, respectively, which resulted in higher HER activity.

Therefore, biaxial tensile strains proves to be a good regulator for bringing the ΔG_H to 0 eV and effectively tune and boost the intrinsic activity of MoS$_2$/graphene hybrid materials with V_S, V_{S2}, V_{MoS3} defects and Mo$_{S2}$ antisite defects. The V_S, V_{S2}, V_{MoS3} defects and Mo$_{S2}$ antisite defects particular had optimal responses in the tensile-strained MoS$_2$/graphene hybrid with optimal ΔG_H values approximately 0 eV. It is indicated that combinations of defect structure and proper strain can significantly improve the HER activity of the MoS$_2$/graphene hybrid material. These combinations were comparatively better than the defect-free MoS$_2$/graphene under biaxial strains condition, which had ΔG_H all larger than 1.60 eV when applying biaxial strains ranging from −5 to +5%. These results indicate that the strain alone is insufficient to activate the basal plane (Fig. 2C).

3.2. Electronic structures of MoS$_2$/graphene system with the different intrinsic defects and baixial strain

To better understand the origin of the different intrinsic defects and strain engineering on the HER mechanism for defective
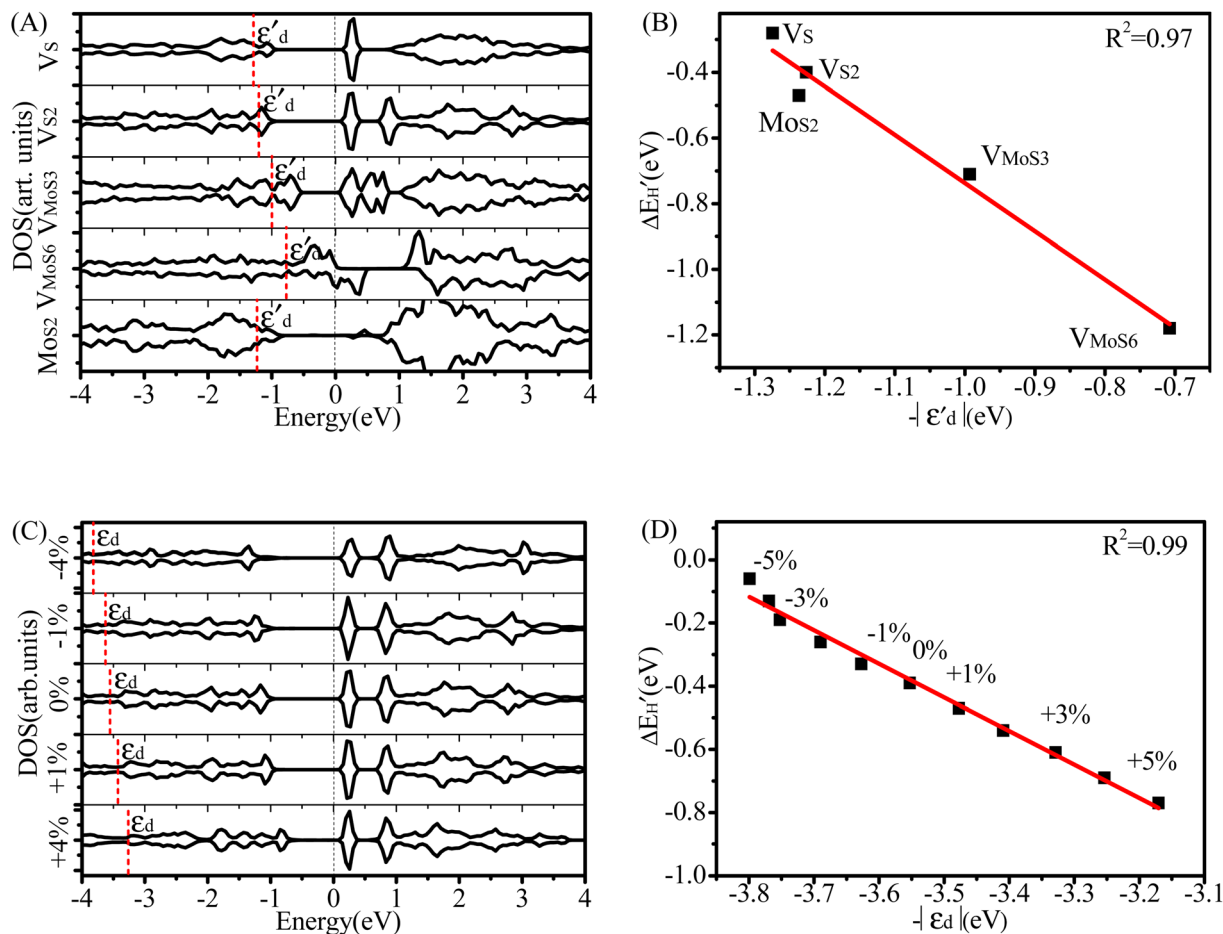
Fig. 4 (A) Spin-polarized densities of states (DOS) projected on 4d states of surface active Mo atoms for MoS$_2$/graphene system with different intrinsic defects: V_S, V_{S2}, V_{MoS3}, V_{MoS6} and Mo$_{S2}$, respectively. The vertical black dashed line indicates the position of the Fermi level, taken as zero energy. (B) Relationship between $\Delta E'_H$ and $-|\varepsilon'_d|$ for various defects: V_S, V_{S2}, V_{MoS3}, V_{MoS6} and Mo$_{S2}$ cases, respectively. (C) Spin-polarized densities of states (DOS) projected on 4d states of surface active Mo atoms for V_{S2}-MoS$_2$/graphene system at different biaxial strains: -4%, -1%, 0%, $+1\%$, $+4\%$, respectively. (D) Relationship between $\Delta E'_H$ and $-|\varepsilon_d|$ for V_{S2}−MoS$_2$/graphene system under -5 to $+5\%$ biaxial strain condition.

MoS$_2$/graphene hybrid materials, we analyzed the electronic structures of these composite materials with intrinsic defects and strain engineering. Firstly, we analyzed the electronic properties of these defective MoS$_2$/graphene systems. The total density of states (TDOS) for MoS$_2$/graphene system with V_S, V_{S2}, V_{MoS3}, V_{MoS6} and Mo$_{S2}$ are investigated, as displayed in Fig. S3.† We observed there are noticeable states appearing near the Fermi level, which is significantly different from the case of defect-free MoS$_2$/graphene system. Since hydrogen atoms directly interact with the Mo site for MoS$_2$/graphene system with V_S, V_{S2}, V_{MoS3}, V_{MoS6} and Mo$_{S2}$ defects, we further focused on the spin-polarized densities of states (DOS) projected on 4d states of surface active Mo atoms that participate in the interaction with the H atom in the MoS$_2$/graphene system with V_S, V_{S2}, V_{MoS3}, V_{MoS6} and Mo$_{S2}$, respectively (Fig. 4A). We can further conclude that the states appearing near the Fermi level is dominated by 4d state of the Mo site. When the H 1s orbital interacts with these new d states, it produces a bonding orbital and an anti-bonding orbital, where the degree of orbitals overlapping near the Fermi level determines the strength of the Mo–H chemical

bonds. To understand this further, we used the d-band center theory of the metals to find an appropriate descriptor by using the d states of Mo atoms to determine the interaction strength. We then plotted the chemical bonding energy between H and the substrate, $\Delta E'_H$, against the value of the d band center, ε_d. The H adsorption energy (ΔE_H) consists of two parts: the chemical bonding energy of H ($\Delta E'_H$), and structural reconstruction energy (ΔE_R), so the chemical bonding energy is defined as $\Delta E'_H = \Delta E_H - \Delta E_R$. The value of ε_d is calculated by following equation:

$$\varepsilon_d = \frac{\int_{-\infty}^{E_F} E\rho(E)\mathrm{d}E}{\int_{-\infty}^{E_F} \rho(E)\mathrm{d}E} \tag{1}$$

As shown in Fig. S4,† $\Delta E'_H$ does not exhibit a good linear correlation with ε_d for defective MoS$_2$/graphene systems with V_S, V_{S2}, V_{MoS3}, V_{MoS6} and Mo$_{S2}$, respectively. However, when we changed the integral energy region to range of -1.5 eV–E_F, named ε'_d, $\Delta E'_H$ displayed a nearly linear relationship with ε'_d for the same five types of defective MoS$_2$/graphene system
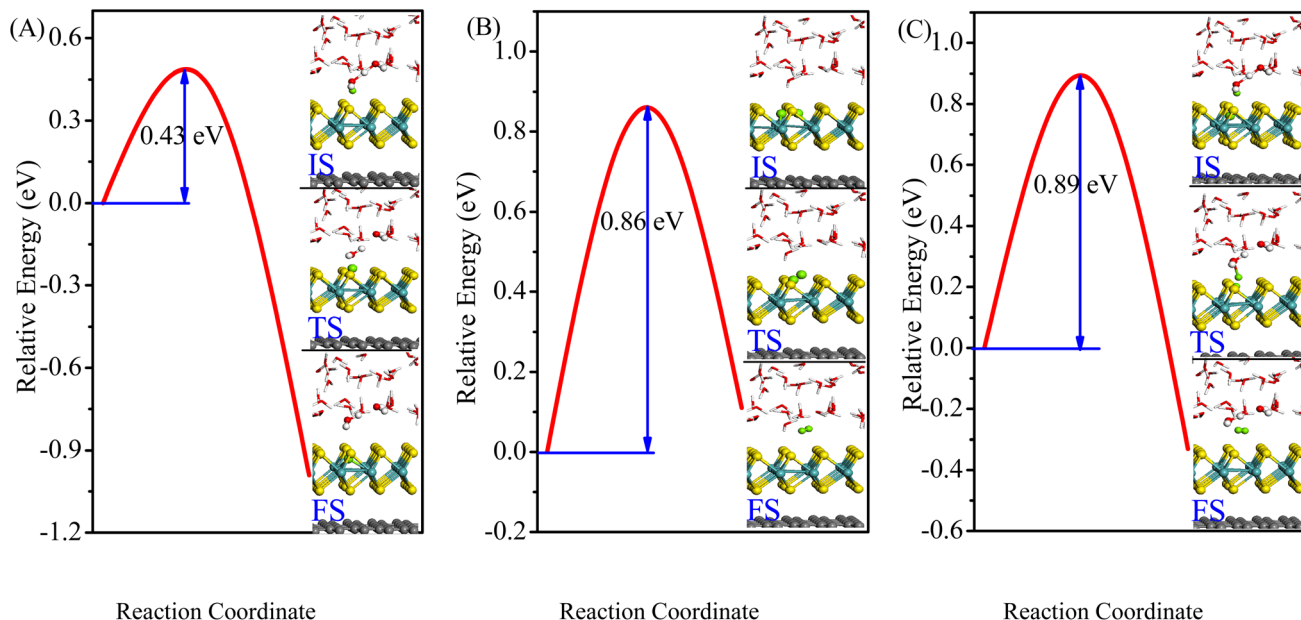
Fig. 5 Minimum-energy pathways of Volmer, Tafel and Heyrovsky reactions on V_{S2}-MoS$_2$/graphene system. The inserts are the corresponding initial state (IS), transition state (TS), and final state (FS).

(Fig. 4B), which indicates that the interaction strength between the H atom and the substrate determined by the Mo-4d state under and near the E_F. As the ε'_d more approaches E_F, the Mo–H bonding more strengthens. While the other two defective MoS$_2$/graphene systems (V_{Mo} and S2$_{Mo}$ defects), the H atom tend to interact directly with S atoms, and would have significant relationships between the S-3p and H-1s states. Therefore, we considered the projected DOS of S-3p state and corresponding integral energy, ε_p (Eqn (1)), which showed a similar H interact with S site. In the same manner, as ε_p more approaches E_F, the S–H bonding more strengthens (Fig. S5†).

Using the V_{S2}-MoS$_2$/graphene system as an example, we next examined the partial DOSs of V_{S2}-MoS$_2$/graphene system at different biaxial strains to understand the mechanism of the variations of ΔG_H tuned by strain engineering, as shown in Fig. 4C. Results show that the introduction of the strain engineering causes a visible shift of the 4d states of the Mo atom directly interacting with adsorbed H atom. The gradually shifts of the Mo-4d state are in excellent agreement with the variation of the biaxial strains. With positive strains (tensile strains), these states gradually shift upwards and move close to the Fermi level, resulting in a gradual strengthening of H binding. These states shift downward and away from the E_F with negative strains (compressive strains), which can clearly explain the weakening of the H interaction with Mo atom in V_{S2}MoS$_2$/graphene. It is suggested that the proper tensile strain tunes the 4d state of the Mo atom, which results in a moderate ΔG_H (Fig. 2B) and higher HER activity. This shows that the strain can be effectively engineered to optimize the hydrogen adsorption strength and achieve ultra-high HER activity. Next, we graphed the relationship between chemical bonding energy, ΔE_{bond}, and the values of d band center, ε_d (Eqn(1)), for V_{S2}–MoS$_2$/graphene system under the biaxial strain condition with a range of −5 to

5% (Fig. 4D) for the purpose of analyzing Mo–H chemical bonds strength variation under the strain engineering. ΔE_{bond} exhibits a nearly linear trend with ε_d of the Mo atom by a coefficient of determination of $R^2 = 0.99$, suggesting that the strength of H binding is actually largely determined by the Mo-4d states. That the emendatory d-band center of metal can provide as an excellent descriptor for determining H adsorption is of great significance, which may pave the way to design ultrahigh-performance MoS$_2$-based HER catalysts.

3.3.   Reaction mechanism analysis

Once we have examined the Gibbs free energy for defective MoS$_2$/Graphene hybrid materials, we next investigated the kinetic energy barriers for H$_2$ revolution using defective V_{S2}-MoS$_2$/Graphene hybrid materials as a representative. The minimum-energy pathways and corresponding initial state (IS), transition state (TS) and final state (FS) are shown in Fig. 5. For HER in acid media, two types of possible pathways have been explored for H$_2$ evolution: Volmer–Heyrovsky or the Volmer–Tafel mechanism. The Volmer reaction is the first step of the HER, in which a hydronium is transferred from the acid solution to a S2 vacancy (H$^+$ + e$^-$ → H$_{ads}$) as shown in Fig. 5A. The calculated barrier (E_a) is 0.43 eV, which is consistent with previous results.[42] The Heyrovsky or Tafel mechanisms were candidates for the second step of the HER process, therefore both barriers of Tafel and Heyrovsky reaction on this active site were explored, as shown in Fig. 5B and C, respectively. In the Tafel step, two adsorbed H atoms reacted to form H$_2$ with a barrier of 0.86 eV, which indicated that electrons could easily form H$_2$ from the adsorbed state. The values of the Tafel reaction for V_{S2}-MoS$_2$/Graphene hybrid materials were much lower than the Mo-edge of a single MoS$_2$ sheet (~1.24 eV) reported in

previous work by Huang.[43] We then predicted activation barrier of 0.89 eV in the Heyrovsky step, where the proton in the water layer reacts with the adsorbed H to form H_2, which is in agreement with the barrier of 0.86 eV estimated from experimental turnover frequency (TOF) for per Mo atom on the Mo edge for hydrogen evolution of MoS_2.[4] The ultralow kinetic barrier both for Volmer–Tafel reaction and Volmer–Heyrovsky reactions suggested that the defective V_{S2}-MoS_2/graphene system exhibits excellent HER kinetic activity.

4. Conclusions

In summary, we have verified two possible approaches to effectively activate the MoS_2 basal plane grown on graphene and greatly improve hydrogen evolution reaction (HER) activity on the basis of first-principles DFT calculation, intrinsic defects and strain engineering simultaneously. We systematically investigated HER activity of MoS_2/graphene hybrid material with seven experimentally produced point defects sites, V_S, V_{S2}, V_{Mo}, V_{MoS3}, V_{MoS6}, Mo_{S2} and $S2_{Mo}$. Our results suggest that four types of those defects (V_S, V_{S2}, Mo_{S2}, V_{MoS3}, respectively) can act as a catalytic active site for HER and exhibit superior electrocatalytic activity. Furthermore, we demonstrated that ΔG_H can be further tuned to an ideal value ($\sim$0 eV) using intrinsic defects and a proper tensile strain simultaneously, which effectively optimizes and boosts the intrinsic HER activity of the active sites, especially for V_S, V_{S2}, V_{MoS3} defects and Mo_{S2} antisite defects under the biaxial tensile strain of 1%, 1%, 4% and 1%, respectively. Interestingly, we found that the emendatory d-band center of metal can serve as an excellent descriptor to determine chemical bonding energy between H and defective MoS_2/graphene hybrid material under different strain condition. Furthermore, the calculated low kinetic barrier of H_2 evolution on the V_{S2}-MoS_2/graphene system indicated that the defective MoS_2/graphene system exhibits excellent HER activity in both the Volmer–Heyrovsky and the Volmer–Tafel mechanisms. Therefore, the methodology of combining intrinsic defect and strain engineering has been shown to be an effective approach for producing a more catalytic active site and improving the HER activity of the MoS_2/graphene hybrid and other two-dimensional materials, which may provide a new way to design ultrahigh-performance MoS_2-based HER catalysts.

Conflicts of interest

There are no conflicts to declare.

Acknowledgements

References

1 J. Deng, H. Li, S. Wang, D. Ding, M. Chen, C. Liu, Z. Tian, K. S. Novoselov, C. Ma, D. Deng and X. Bao, *Nat. Commun.*, 2017, **8**, 14430.

2 H. Duan, C. Wang, G. Li, H. Tan, W. Hu, L. Cai, W. Liu, N. Li, Q. Ji, Y. Wang, Y. Lu, W. Yan, F. Hu, W. Zhang, Z. Sun, Z. Qi, L. Song and S. Wei, *Angew. Chem., Int. Ed.*, 2021, **60**, 7251–7258.

3 B. Hinnemann, P. G. Moses, J. Bonde, K. P. Jørgensen, J. H. Nielsen, S. Horch, I. Chorkendorff and J. K. Nørskov, *J. Am. Chem. Soc.*, 2005, **127**, 5308–5309.

4 J. Chen, G. Liu, Y. Zhu, M. Su, P. Yin, X. Wu, Q. Lu, C. Tan, M. Zhao, Z. Liu, W. Yang, H. Li, G. Nam, L. Zhang, Z. Chen, X. Huang, P. M. Radjenovic, W. Huang, Z. Tian, J. Li and H. Zhang, *J. Am. Chem. Soc.*, 2020, **142**, 7161–7167.

5 X. Zhang, S. Hua, L. Lai, Z. Wang, T. Liao, L. He, H. Tang and X. Wan, *RSC Adv.*, 2022, **12**, 17959–17983.

6 S. Han, X. Li, X. Zeng, D. Cao and J. Chen, *Int. J. Hydrogen Energy*, 2022, **47**, 37850–37859.

7 J. Xie, H. Zhang, S. Li, R. Wang, X. Sun, M. Zhou, J. Zhou, X. Lou and Y. Xie, *Adv. Mater.*, 2013, **25**, 5807–5813.

8 M. Remskar, A. Mrzel, Z. Skraba, A. Jesih, M. Ceh, J. Demsar, P. Stadelmann, F. Levy and D. Mihailovic, *Science*, 2001, **292**, 479–481.

9 Y. Li, H. Wang, L. Xie, Y. Liang, G. Hong and H. Dai, *J. Am. Chem. Soc.*, 2011, **133**, 7296–7299.

10 A. Hasani, M. Tekalgne, Q. V. Le, H. W. Jang and S. Y. Kim, *J. Mater. Chem. A*, 2019, **7**, 430–454.

11 C. Gabbett, C. S. Boland, A. Harvey, V. Vega-Mayoral, R. J. Young and J. N. Coleman, *Chem. Mater.*, 2018, **30**, 5245–5255.

12 D. Voiry, R. Fullon, J. C. Yang, C. de Carvalho Castro e Silva, R. Kappera, I. Bozkurt, D. Kaplan, M. J. Lagos, P. E. Batson, G. Gupta, A. D. Mohite, L. Dong, D. Er, V. B. Shenoy, T. Asefa and M. Chhowalla, *Nat. Mater.*, 2016, **15**, 1003.

13 X. Xu, Z. Peng, H. Xu and D. Cheng, *J. Catal.*, 2022, **416**, 47–57.

14 X. Wang, Y. Zhang, H. Si, Q. Zhang, J. Wu, L. Gao, X. Wei, Y. Sun, Q. Liao, Z. Zhang, K. Ammarah, L. Gu, Z. Kang and Y. Zhang, *J. Am. Chem. Soc.*, 2020, **142**, 4298–4308.

15 C. Tsai, H. Li, S. Park, J. Park, H. Soo Han, J. K. Nørskov, X. Zheng and F. Abild-Pedersen, *Nat. Commun.*, 2017, **10**, 1038.

16 L. Wang, Z. Zeng, W. Gao, T. Maxson, D. Raciti, M. Giroux, X. Pan, C. Wang and J. Greeley, *Science*, 2019, **363**, 870–874.

17 M. Escudero-Escribano, P. Malacrida, M. H. Hansen, U. G. Vej-Hansen, A. Velázquez- Palenzuela, V. Tripkovic, J. Schiøtz, J. Rossmeisl, I. E. L. Stephens and I. Chorkendorff, *Science*, 2016, **352**, 73–76.

18 S. Maiti, K. Maiti, M. T. Curnan, K. Kim, K. Noh and J. W. Han, *Energy Environ. Sci.*, 2021, **14**, 3717–3756.

19 D. B. Putungan, S. H. Lin and J. L. Kuo, *Phys. Chem. Chem. Phys.*, 2015, **17**, 21702–21708.

20 H. Li, C. Tsai, A. L. Koh, L. Cai, A. W. Contryman, A. H. Fragapane, J. Zhao, H. S. Han, H. C. Manoharan,

F. Abildpedersen, J. K. Nørskov and X. Zheng, *Nat. Mater.*, 2016, **15**, 48–53.

21 N. Dimakis, S. Gupta, R. Wadud and M. I. Bhatti, *Comput. Mater. Sci.*, 2022, **205**, 111234.

22 N. Dimakis, S. Gupta, R. Wadud and M. I. Bhatti, *Data Brief*, 2022, **42**, 108054.

23 W. Zhou, X. Zou, S. Najmaei, Z. Liu, Y. Shi, J. Kong, J. Lou, P. M. Ajayan, B. I. Yakobson and J. C. Idrobo, *Nano Lett.*, 2013, **13**, 2615–2622.

24 J. Hong, Z. Hu, M. Probert, K. Li, D. Lv, X. Yang, L. Gu, N. Mao, Q. Feng and L. Xie, *Nat. Commun.*, 2015, **6**, 6293.

25 P. Joensen, E. D. Crozier, N. Alberding and R. F. Frindt, *J. Phys. C: Solid State Phys.*, 1987, **20**, 4043.

26 D. Le, T. B. Rawal and T. S. Rahman, *J. Phys. Chem. C*, 2014, **118**, 5346–5351.

27 C. Ataca and S. Ciraci, *J. Phys. Chem. C*, 2011, **115**, 13303–13311.

28 S. Plimpton, *J. Comput. Phys.*, 1995, **117**, 1–19.

29 P. K. Yuet and B. Daniel, *J. Phys. Chem. B*, 2010, **114**, 13786–13795.

30 M. Heiranian, Y. B. Wu and N. R. Alurub, *J. Chem. Phys.*, 2017, **147**, 104706.

31 R. W. Hockney and J. W. Eastwood, *Computer Simulation Using Particles*, Taylor & Francis, Inc., 1988.

32 G. Kresse and J. Hafner, *Phys. Rev. B: Condens. Matter Mater. Phys.*, 1993, **47**, 558–561.

33 G. Kresse and J. Hafner, *Phys. Rev. B: Condens. Matter Mater. Phys.*, 1994, **49**, 14251–14269.

34 G. Kresse and J. Furthmüller, *Phys. Rev. B: Condens. Matter Mater. Phys.*, 1996, **54**, 11169–11189.

35 P. E. Blöchl, *Phys. Rev. B: Condens. Matter Mater. Phys.*, 1994, **5**, 17953–17979.

36 J. P. Perdew, K. Burke and M. Ernzerhof, *Phys. Rev. Lett.*, 1997, **78**, 1396.

37 S. Grimme, J. Antony, S. Ehrlich and H. Krieg, *J. Chem. Phys.*, 2010, **132**, 154104.

38 P. Atkins, *Physical Chemistry*, Oxford University Press, Oxford, U.K., 10th edn, 2014, pp. 1–1008.

39 G. Henkelman, B. P. Uberuaga and H. Jónsson, *J. Chem. Phys.*, 2000, **113**, 9901–9904.

40 B. Hinneman, P. G. Moses, J. Bonde, K. P. Jørgensen, J. H. Nielsen, S. Horch, I. Chorkendorff and J. K. Nørskov, *J. Am. Chem. Soc.*, 2005, **127**, 5308–5309.

41 C. Tsai, K. Chan, J. K. Nørskov and F. Abild-Pedersen, *Surf. Sci.*, 2015, **640**, 133–140.

42 S. Chen, X. Chen, G. Wang, L. Liu, Q. He, X. B. Li and N. Cui, *Chem. Mater.*, 2018, **30**, 5404–5411.

43 Y. Huang, R. J. Nielsen, W. A. Goddard and M. P. Soriaga, *J. Am. Chem. Soc.*, 2015, **137**, 6692–6698.